

IMAGE PROCESSING AND ENHANCEMENT

Medical images acquired in most radiological applications are visually examined by a physician. The purpose of image enhancement methods is to process an acquired image for better contrast and visibility of features of interest for visual examination as well as subsequent computer-aided analysis and diagnosis. As described in Chapters 4–7, different medical imaging modalities provide specific information about internal organs or biological tissues. Image contrast and visibility of the features of interest depend on the imaging modality as well as the anatomical regions.

There is no unique general theory or method for processing all kinds of medical images for feature enhancement. Specific medical imaging applications (such as cardiac, neurological, and mammography) present different challenges in image processing for feature enhancement and analysis. Medical images show characteristic information about the physiological properties of the structures and tissues. However, the quality and visibility of information depends on the imaging modality and the response functions (such as the point spread function [PSF]) of the imaging scanner. Medical images from specific modalities need to be processed using a method that is suitable to enhance the features of interest. For example, a chest X-ray radiographic image shows the anatomical structure of the chest based on the total attenuation coefficients. If the radiograph is being examined for a possible fracture in the ribs, the image enhancement method is required to improve the visibility of hard bony structures. But if an X-ray mammogram is obtained for examination of potential breast cancer, an image processing method is required to enhance visibility of microcalcifications, speculated masses, and soft-tissue structures such as parenchyma. A single image enhancement method may not serve both of these applications. Image enhancement methods for improving the soft tissue contrast in magnetic resonance (MR) brain images may be entirely different from those used for positron emission tomography (PET) brain images. Thus, image enhancement tasks and methods are very much application-dependent.

Image enhancement methods may also include image restoration methods, which are generally based on minimum mean-squared error operations, such as Wiener filtering and other constrained deconvolution methods incorporating some *a priori* knowledge of degradation (1–5). Since the main objective is to enhance

features of interest, a suitable combination of both restoration and contrast enhancement algorithms is the integral part of preprocessing in image analysis. The selection of a specific restoration algorithm for noise removal is highly dependent on the image acquisition system. For example, in the filtered-backprojection method for reconstructing images in computed tomography (CT), the raw data obtained from the scanner is first deconvolved with a specific filter. Filter functions such as Hamming window, as described in Chapter 8, may also be used to reduce noise in the projection data. On the other hand, several image enhancement methods, such as neighborhood-based operations and frequency filtering operations, implicitly de-emphasize noise for feature enhancement.

Image enhancement tasks are usually characterized in two categories (1–5):

1. **Spatial Domain Methods:** These methods manipulate image pixel values in the spatial domain based on the distribution statistics of the entire image or local regions. Histogram transformation, spatial filtering, region-growing, morphological image processing, and model-based image estimation methods are some examples in this category of image and feature enhancement.
2. **Frequency Domain Methods:** These methods manipulate information in the frequency domain based on the frequency characteristics of the image. Frequency filtering, homomorphic filtering, and wavelet processing methods are some examples in this category of frequency representation-based image and feature enhancement.

In addition to the above general approaches for image and feature enhancement, model-based techniques such as Hough transform, matched filtering, neural networks, and knowledge-based systems are also used to extract specific features for pattern recognition and classification. These methods are discussed in detail in the next chapter.

9.1. SPATIAL DOMAIN METHODS

Spatial domain methods process an image with pixel-by-pixel transformation based on the histogram statistics or neighborhood operations. These methods are usually faster in computer implementation as compared to frequency filtering methods that require computation of Fourier transform for frequency domain representation. However, frequency filtering methods may provide better results in some applications if a priori information about the characteristic frequency components of the noise and features of interest is available. For example, specific spike degradations due to mechanical stress and vibration on the gradient coils in the raw signal often cause striation artifacts in fast MR imaging techniques. The spike degradation-based noise in the MR signal can be modeled with their characteristic frequency components and can be removed by selective filtering and wavelet processing methods (7). Wiener filtering methods have been applied for signal enhancement to remove frequency components related to the undesired resonance effects of the nuclei and noise suppression in MR imaging (8–10).

9.1.1 Histogram Transformation and Equalization

A histogram of an image provides information about the intensity distribution of pixels in the image. The simplest form of a histogram is the plot of occurrence of specific gray-level values of the pixels in the image. For example, there are 256 gray levels ranging from 0 to 255 in an image with 8-bit gray-level resolution. The occurrence of gray levels can be provided in terms of the absolute values, that is, the number of times a specific gray level has occurred in the image, or the probability values, that is, the probability of occurrence of a specific gray level in the image. In mathematical terms, a histogram $h(r_i)$ is expressed as

$$h(r_i) = n_i \quad \text{for } i = 0, 1, \dots, L - 1 \quad (9.1)$$

where r_i is the i th gray level in the image for a total of L gray values and n_i is the number of occurrences of gray-level r_i in the image.

If a histogram is expressed in terms of the probability of occurrence of gray levels, it can be expressed as

$$p_r(r_i) = \frac{n_i}{n} \quad (9.2)$$

where n is the total number of pixels in the image.

Thus, a histogram is a plot of $h(r_i)$ or $p_r(r_i)$ versus r_i . Figure 9.1 shows X-ray CT and T_2 -weighted proton density MR images of brain with their respective histogram $h(r_i)$.

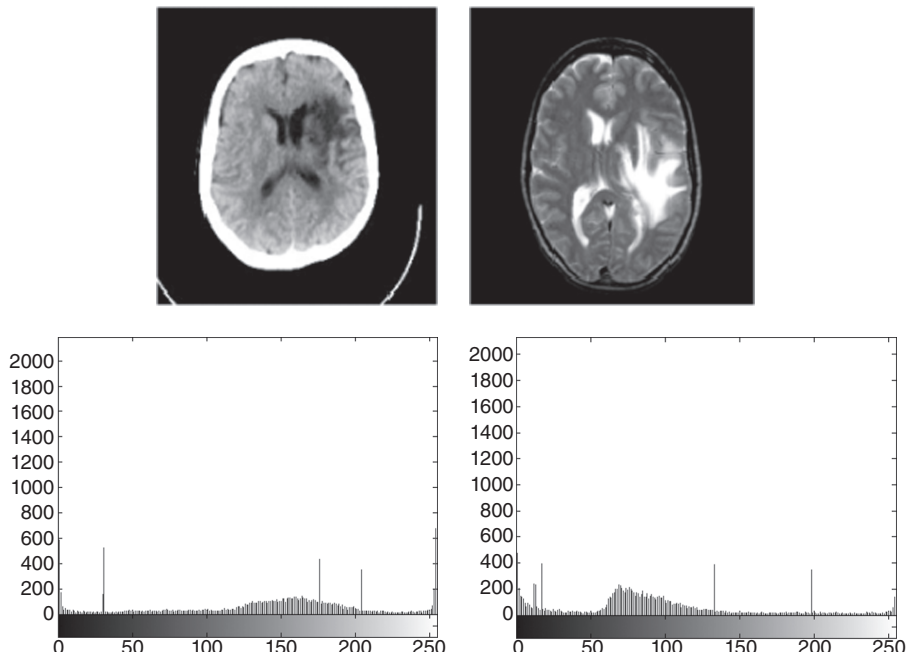


Figure 9.1 An X-ray CT image (top left) and T_2 -weighted proton density image (top right) of human brain cross-sections with their respective histograms at the bottom.

A histogram can be scaled linearly to change the dynamic range of gray levels in the image. Let us assume that an image has all of its gray levels in the range $[a, b]$ where the minimum gray level is represented by a and the maximum gray level value is given by b . The utilization of dynamic range of gray levels in the image can be seen in the histogram. Using a histogram scaling method, the gray level range of $[a, b]$ can be changed to a new gray level range of $[c, d]$ by a linear transformation as

$$z_{\text{new}} = \frac{d - c}{b - a} (z - a) + c \quad (9.3)$$

where z and z_{new} are, respectively, the original and new gray-level values of a pixel in the image.

If an image is not using the full dynamic range of gray levels (e.g., 256 gray levels from 0 to 255 for an image with 8-bit gray level resolution), a histogram scaling method can be used to expand the dynamic range to its full possible range to improve the contrast and brightness in general. An example of image histogram scaling is shown in Figure 1.8 in Chapter 1.

A popular general-purpose method of image enhancement is histogram equalization. In this method, a monotonically increasing transformation function, $T(r)$, is used to map the original gray values, r_i of the input image, into new gray values, s_i of the output image, such that

$$\begin{aligned} s_i &= T(r_i) = \sum_{j=0}^i p_r(r_j) \\ &= \sum_{j=0}^i \frac{n_j}{n} \quad \text{for } i = 0, 1, \dots, L-1 \end{aligned} \quad (9.4)$$

where $p_r(r_i)$ is the probability-based histogram of the input image that is transformed into the output image with the histogram $p_s(s_i)$.

The transformation function $T(r_i)$ in Equation 9.4 stretches the histogram of the input image such that the gray values occur in the output image with equal probability of occurrence. It should be noted that the uniform distribution of the histogram of the output image is limited by discrete computation of the gray-level transformation. The histogram equalization method forces image intensity levels to be redistributed with an equal probability of occurrence.

Figure 9.2 shows the enhanced images of the brain images shown in Figure 9.1 as obtained by the histogram equalization method. The respective histograms of the enhanced images are shown at the bottom.

The histogram equalization method stretches the contrast of an image by redistributing the gray values to achieve a uniform distribution. This general method may not provide good results in many applications. The histogram equalization method may cause saturation in some regions of the image resulting in loss of details and high-frequency information that may be necessary for interpretation. Sometimes, local histogram equalization is applied separately on predefined local neighborhood regions, such as 7×7 pixels, to provide better results (1).

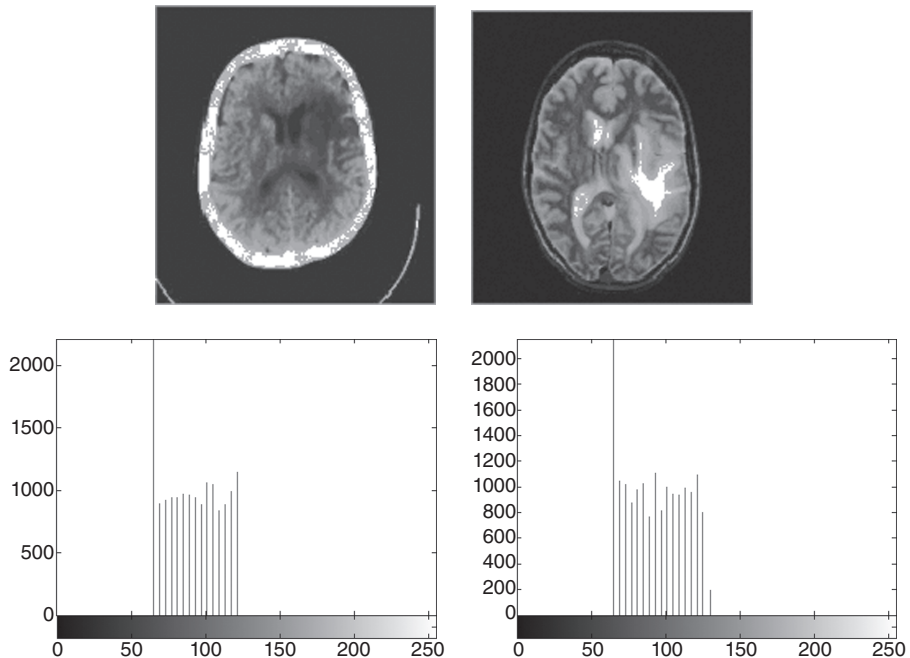


Figure 9.2 Histogram equalized images of the CT and MR brain images shown in Figure 9.1 (top) and their respective histograms (bottom).

9.1.2 Histogram Modification

If a desired distribution of gray values is known a priori, a histogram modification method is used to apply a transformation that changes the gray values to match the desired distribution. The target distribution can be obtained from a good contrast image that is obtained under similar imaging conditions. Alternatively, an original image from a scanner can be interactively modified through regional scaling of gray values to achieve the desired contrast. This image can now provide a target distribution to the rest of the images, obtained under similar imaging conditions, for automatic enhancement using the histogram modification method.

Let us assume that $p_z(z_i)$ is the target histogram expressed, and $p_r(r_i)$ and $p_s(s_i)$ are, respectively, the histograms of the input and output image. A transformation is needed such that the output image $p_s(s_i)$ should have the desired histogram of $p_z(z_i)$. The first step in this process is to equalize $p_r(r_i)$ using the Equation 9.3 such that (1, 6)

$$u_i = T(r_i) = \sum_{j=0}^i p_r(r_j) \quad \text{for } i = 0, 1, \dots, L-1 \quad (9.5)$$

where u_i represents the equalized gray values of the input image.

A new transformation V is defined to equalize the target histogram such that

$$u_i = V(z_i) = \sum_{k=0}^i p_z(z_k) \quad \text{for } i = 0, 1, \dots, L-1. \quad (9.6)$$

Putting $V(z_i) = T(r_i) = u_i$ to achieve the target distribution, new gray values s_i for the output image are computed from the inverse transformation V^{-1} as

$$s_i = z_i = V^{-1}[T(r_i)] = V^{-1}(u_i). \quad (9.7)$$

With the transformation defined in Equation 9.7, the histogram distribution of the output image $p_s(s_i)$ would become similar to the target histogram $p_z(z_i)$.

9.1.3 Image Averaging

Signal averaging is a well-known method for enhancing signal-to-noise ratio (SNR). In medical imaging, data from the detector is often averaged over time or space for signal enhancement. However, such signal enhancement is achieved at the cost of some loss of temporal or spatial resolution. Sequence images, if properly registered and acquired in nondynamic applications, can be averaged for noise reduction leading to smoothing effects. Selective weighted averaging can also be performed over a specified neighborhood of pixels in the image.

Let us assume that an ideal image $f(x, y)$ is degraded by the presence of additive noise $n(x, y)$. The acquired image $g(x, y)$ then can be represented as

$$g(x, y) = f(x, y) + n(x, y). \quad (9.8)$$

In a general imaging process, the noise is assumed to be uncorrelated and random with a zero average value. If a sequence of K images is acquired for the same object under the same imaging conditions, the average image $\bar{g}(x, y)$ can be obtained as

$$\bar{g}(x, y) = \frac{1}{K} \sum_{i=1}^K g_i(x, y) \quad (9.9)$$

where $g_i(x, y); i = 1, 2, \dots, K$ represents the sequence of images to be averaged.

As the number of images K increases, the expected value of the average image $\bar{g}(x, y)$ approaches to $f(x, y)$, reducing the noise per pixel in the averaged image as

$$\begin{aligned} E\{\bar{g}(x, y)\} &= f(x, y) \\ \sigma_{\bar{g}(x, y)} &= \frac{1}{\sqrt{K}} \sigma_{n(x, y)} \end{aligned} \quad (9.10)$$

where σ represents the standard deviation of the respective random field.

9.1.4 Image Subtraction

If two properly registered images of the same object are obtained with different imaging conditions, a subtraction operation on the acquired image can enhance the information about the changes in imaging conditions. This simple enhancement method is applied in angiography where an image of the anatomy with vascular structure is obtained first. An appropriate dye or tracer drug is then administered in the body and flows through the vascular structure. A second image is acquired of the same anatomy at the peak of the tracer flow. The subtraction of these two images then produces an image with good contrast and visibility of the vascular structure. Figure 9.3 shows an MR angiographic image obtained using the subtraction method.

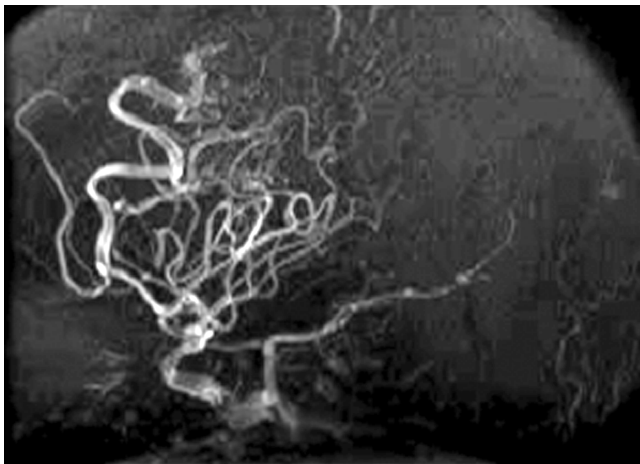


Figure 9.3 An MR angiography image obtained through image subtraction method.

	$f(x-1,y)$			$f(x-1,y-1)$	$f(x-1,y)$	$f(x-1,y+1)$
$f(x,y-1)$	$f(x,y)$	$f(x,y+1)$		$f(x,y-1)$	$f(x,y)$	$f(x,y+1)$
	$f(x+1,y)$			$f(x+1,y-1)$	$f(x+1,y)$	$f(x+1,y+1)$

Figure 9.4 A 4-connected (left) and 8-connected neighborhood of a pixel $f(x, y)$.

9.1.5 Neighborhood Operations

The spatial filtering methods using neighborhood operations involve the convolution of the input image with a specific mask (such as Laplacian-based high-frequency emphasis filtering mask) to enhance an image. The gray value of each pixel is replaced by the new value computed according to the mask applied in the neighborhood of the pixel. The neighborhood of a pixel may be defined in any appropriate manner based on a simple connectedness or any other adaptive criterion (13). Figure 9.4 shows 4- and 8-connected neighborhoods of a central pixel in 3×3 pixel regions.

A weight mask is first created by assigning weights for each pixel location in the selected type of neighborhood. The weight mask is then convolved with the image. With an appropriate design of the mask, specific operations including image smoothing and enhancement can be performed. For example, using a Laplacian weight mask, edge features can be emphasized in the enhanced image.

Let us assume a general weight mask of $(2p + 1) \times (2p + 1)$ pixels where p can take integer values, such as 1, 2, ..., depending on the size of the mask. For $p = 1$, the size of the weight mask is 3×3 pixels. A discrete convolution of an image $f(x, y)$ with a spatial filter represented by a weight mask $w(x, y)$ is given by

1	2	1
2	4	2
1	2	1

Figure 9.5 A weighted averaging mask for image smoothing. The mask is used with a scaling factor of 1/16 that is multiplied to the values obtained by convolution of the mask with the image (Eq. 9.11).

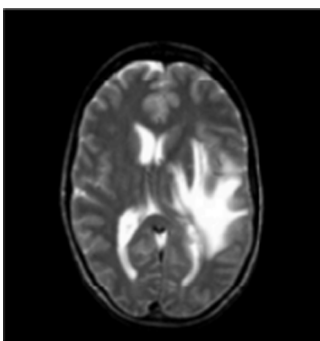


Figure 9.6 Smoothed image of the MR brain image shown in Figure 9.1 as a result of the spatial filtering using the weighted averaging mask shown in Figure 9.5.

$$g(x, y) = \frac{1}{\sum_{x'=-p}^p \sum_{y'=-p}^p w(x', y')} \sum_{x'=-p}^p \sum_{y'=-p}^p w(x', y') f(x+x', y+y'). \quad (9.11)$$

The convolution in Equation 9.11 is performed for all values of x and y in the image. In other words, the weight mask of the filter is translated and convolved over the entire extent of the input image to provide the output image.

The values of the weight mask are derived from a discrete representation of the selected filter. Based on the filter, the characteristics of the input image are changed in the output image. For example, Figure 9.5 shows a weighted averaging mask that can be used for image smoothing and noise reduction. In this mask, the locations of pixels in the 4-connected neighborhood are weighted two times more than other pixels. The reason is that pixels in the 4-connected neighborhood are closer than others to the central pixel. Figure 9.6 shows the MR brain image smoothed by spatial filtering using the weighted averaging mask shown in Figure 9.5 on the image shown in Figure 9.1. Some loss of details can be noted in the smoothed image because of the averaging operation. To minimize the loss of details, an adaptive median filtering may be applied (1–4).

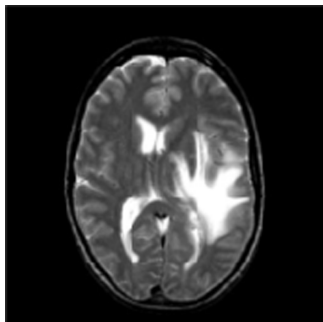


Figure 9.7 A smoothed MR brain image obtained by spatial filtering using the median filter method over a fixed neighborhood of 3×3 pixels.

9.1.5.1 Median Filter Median filter is a well-known order-statistics filter that replaces the original gray value of a pixel by the median of gray values of pixels in the specified neighborhood. For example, for 3×3 pixels-based fixed neighborhood (Fig. 9.4), the gray value of the central pixel $f(x, y)$ is replaced by the median of gray values of all 9 pixels in the neighborhood. Instead of replacing the gray value of the central pixel by the median operation of the neighborhood pixels, other operations such as midpoint, arithmetic mean, and geometric mean can also be used in order-statistics filtering methods (1–5). A median filter operation for a smoothed image $\hat{f}(x, y)$, computed from the acquired image $g(x, y)$, is defined as

$$\hat{f}(x, y) = \underset{(i, j) \in N}{\text{median}} \{g(i, j)\} \quad (9.12)$$

where N is the prespecified neighborhood of the pixel (x, y) .

Figure 9.7 shows the smoothed MR brain image as obtained by median filtering over the neighborhoods of 3×3 pixels. Adaptive neighborhoods can be used for median filtering to preserve the edges better. Several methods of adaptive neighborhoods are used in the literature including fixed shape and feature adaptive neighborhoods (1, 13). In adaptive neighborhood processing, a region centered at a pixel is grown until a prespecified criterion of region growing is satisfied. One simple method of region growing is to grow a neighborhood around the central pixel from 3×3 pixels to 5×5 pixels and so on, until the difference between the gray value of the central pixel and the average of all other pixels in the neighborhood is within a preselected threshold. Thus, local neighborhoods with different sizes can be used for median filtering for preserving edge details in the smoothed image.

9.1.5.2 Adaptive Arithmetic Mean Filter Adaptive local noise-reduction filtering can be applied using the variance information of the selected neighborhood and an estimate of the overall variance of noise in the image. If the noise variance of the image is similar to the variance of gray values in the specified neighborhood of pixels, the filter provides an arithmetic mean value of the neighborhood. Let σ_n^2 be an estimate of the variance of the noise in the image and σ_s^2 be the variance of gray values of pixels in the specified neighborhood. An adaptive local noise-reduction filtering can be implemented as

$$\hat{f}(x, y) = g(x, y) - \frac{\sigma_n^2}{\sigma_s^2} [g(x, y) - \bar{g}_{ms}(x, y)] \quad (9.13)$$

where $\bar{g}_{ms}(x, y)$ is the mean of the gray values of pixels in the specified neighborhood.

It should be noted that if the noise variance is zero in the image, the resultant image is the same as the input image. If an edge were present in the neighborhood, the local variance would be higher than the noise variance of the image. In such cases, the above estimate in Equation 9.13 would return the value close to the original gray value of the central pixel.

9.1.5.3 Image Sharpening and Edge Enhancement Edges in an image are basically defined by the change in gray values of pixels in the neighborhood. The change of gray values of adjacent pixels in the image can be expressed by a derivative (in continuous domain) or a difference (in discrete domain) operation.

A first-order derivative operator, such as Sobel, computes the gradient information in a specific direction. The derivative operator can be encoded into a weight mask. Figure 9.8 shows two Sobel weight masks that are used, respectively, in computing the first-order gradient in x - and y -directions (defined by $\frac{\partial f(x, y)}{\partial x}$ and $\frac{\partial f(x, y)}{\partial y}$). These weight masks of 3×3 pixels each are used for convolution to compute respective gradient images. For spatial image enhancement based on the first-order gradient information, the resultant gradient image can simply be added to the original image and rescaled using the full dynamic range of gray values. Four weight masks to compute directional first-order gradients are shown in Figure 9.9. These masks compute gradient in, respectively, horizontal, 45-degree vertical, and 135-degree directions. The gradient information thus obtained can be further used for specific directional feature enhancement and extraction for image segmentation (discussed in the next chapter).

A second-order derivative operator, known as Laplacian, can be defined as

$$\begin{aligned} \nabla^2 f(x, y) &= \frac{\partial^2 f(x, y)}{\partial x^2} + \frac{\partial^2 f(x, y)}{\partial y^2} \\ &= [f(x+1, y) + f(x-1, y) + f(x, y+1) + f(x, y-1) - 4f(x, y)] \end{aligned} \quad (9.14)$$

-1	-2	-1
0	0	0
1	2	1

-1	0	1
-2	0	2
-1	0	1

Figure 9.8 Weight masks for first-order derivative-based Sobel operator. The mask at the left is for computing gradient in the x -direction while the mask at the right computes the gradient in the y -direction.

-1	-1	-1
0	0	0
1	1	1

-1	0	1
-1	0	1
-1	0	1

-1	-1	0
-1	0	1
-0	1	1

0	1	1
-1	0	1
-1	-1	0

Figure 9.9 Weight masks for computing first-order gradient in (clockwise from top left) in horizontal, 45-degree, vertical, and 135-degree directions.

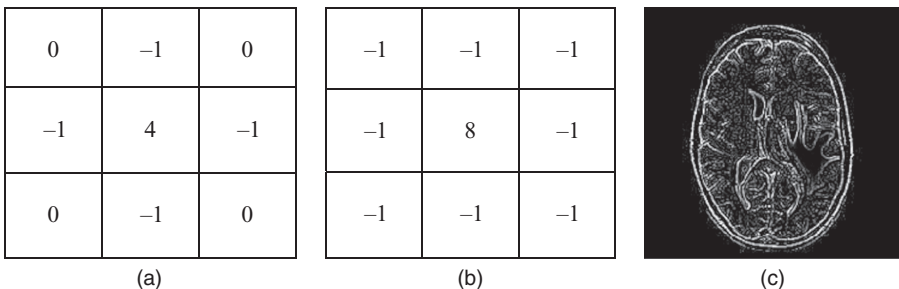


Figure 9.10 (a) A Laplacian weight mask using 4-connected neighborhood pixels only; (b) a Laplacian weight mask with all neighbors in a window of 3×3 pixels; and (c) the resultant second-order gradient image obtained using the mask in (a).

where $\nabla^2 f(x, y)$ represents the second-order derivative or Laplacian of the image $f(x, y)$.

A Laplacian mask with diagonal neighbors is shown in Figure 9.10 with the resultant MR brain image showing edge as obtained by spatial filtering convolving the MR brain image shown in Figure 9.1 with this mask. Adding the Laplacian (edge information) to the image provides a simple method of edge-based image enhancement. This can be accomplished by changing the weight value of the central location in the mask from 8 to 9. A different value can be assigned to this location to change the relative emphasis of edges to the image. Figure 9.11 shows the weight mask- and edge-based image enhancement of the same image.

9.1.5.4 Feature Enhancement Using Adaptive Neighborhood Processing

An automated gray-level remapping method for enhancement of details in chest

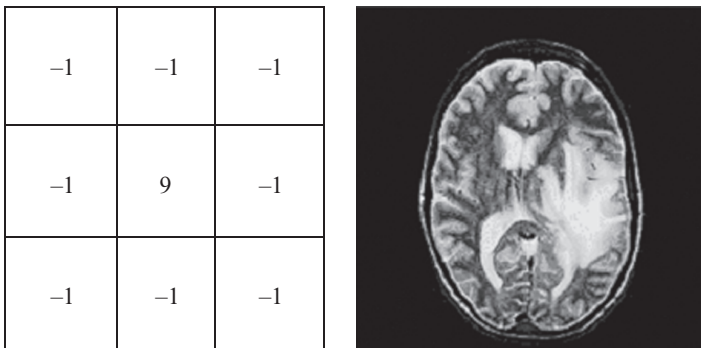


Figure 9.11 Laplacian-based image-enhancement weight mask with diagonal neighbors and the resultant enhanced image with emphasis on second-order gradient information.

region CT images was used by Davis and Wallenslager (11). The objective of this enhancement is to reduce dark line artifacts in CT chest images and to provide an aid to the automatic detection of the lung region. Pizer et al. (12) developed an adaptive gray-level assignment method for CT image enhancement. Dhawan et al. (13) used an adaptive neighborhood-based image processing technique that utilizes a low-level analysis and knowledge about desired features in designing a contrast enhancement function. The contrast enhancement function (CEF) is then used to enhance mammographic features while suppressing the noise. In this method, an adaptive neighborhood structure is defined as a set of two neighborhoods: inner and outer. Three types of adaptive neighborhoods can be defined: constant ratio, constant difference, and feature adaptive. A constant ratio adaptive neighborhood criterion is one that maintains the ratio of the inner to outer neighborhood size at 1:3, that is, each adaptive neighborhood around a pixel had an inner neighborhood of size $c \times c$ and an outer neighborhood of size $3c \times 3c$, where c is an odd number. A constant difference neighborhood criterion is the one that allows the size of the outer neighborhood to be $(c + n) \times (c + n)$, where n is a positive even integer. Note that both of the above mentioned neighborhoods are of fixed shape, that is, square. These neighborhoods can only provide the closest possible approximation of the local features into square regions. However, mammographic features are of arbitrary shape and are highly variable in shape and size. The approximation of local features into square regions may cause loss of fine details about these features.

A variable shaped feature adaptive neighborhood criterion that adapts the arbitrary shape and size of the local features to obtain the “center” (consisting of pixels forming the feature) and the “surround” (consisting of pixels forming the background for that feature) regions is defined using the predefined similarity and distance criteria. These regions are used to compute the local contrast for the centered pixel. The procedure to obtain the center and the surround regions is as follows.

1. The inner and outer neighborhoods around a pixel are grown using the constant difference adaptive neighborhood criterion. To define the similarity criterion, gray-level and percentage thresholds are defined. For example, a gray level

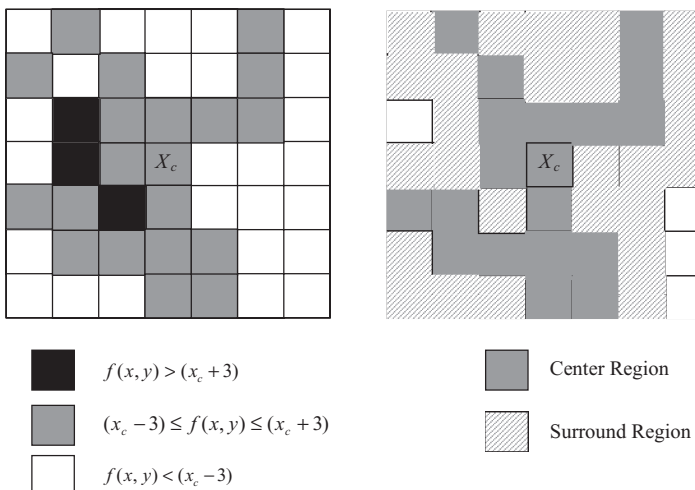


Figure 9.12 Region growing for a feature adaptive neighborhood: image pixel values in a 7×7 neighborhood (left) and central and surround regions for the feature-adaptive neighborhood.

threshold of 3 and a percentage threshold of 60 are used in Figure 9.12. Using these thresholds, the region around each pixel in the image is grown in all the directions until the similarity criterion is violated. At the point of violation, the region forming all pixels, which have been included in the neighborhood of the centered pixel satisfying the similarity criterion, are designated as the center region. The surround region is then computed using the distance criterion, which may be a unit distance in all directions (Fig. 9.12). Thus, the surround region is comprised of all pixels contiguous to the center region. The local contrast $C(x, y)$ for the centered pixel is then computed as

$$C(x, y) = \frac{|P_c(x, y) - P_s(x, y)|}{\max \{P_c(x, y), P_s(x, y)\}} \quad (9.15)$$

where $P_c(x, y)$ and $P_s(x, y)$ are the average gray-level values of the pixels corresponding to the center and the surround regions, respectively, centered on the pixel.

2. The CEF is used as a function to modify the contrast distribution in the contrast domain of the image. A contrast histogram is computed as a tool for controlling the efficiency and the performance of the algorithm. The contrast histogram is the plot of occurrence of contrast levels (discretized with a suitable degree of resolution) in the contrast domain. The contrast histogram is analyzed and correlated to the requirements of feature enhancement, such as microclassification enhancement. Using the CEF, a new contrast value, $C'(x, y)$, is computed.
3. The new contrast value $C'(x, y)$ is used to compute a new pixel value for the enhanced image $g(x, y)$ as

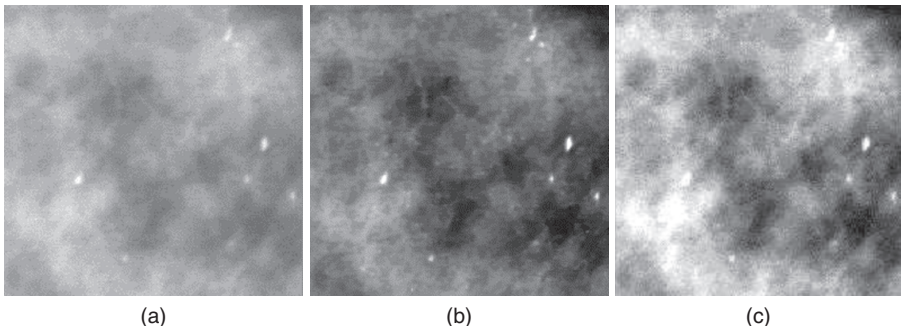


Figure 9.13 (a) A part of a digitized breast film-mammogram with microcalcification areas. (b) Enhanced image through feature adaptive contrast enhancement algorithm. (c) Enhanced image through histogram equalization method.

$$g(x, y) = \begin{cases} \frac{P_s(x, y)}{1 - C'(x, y)} & \text{if } P_c(x, y) \geq P_s(x, y) \\ g(x, y) = P_s(x, y)(1 - C'(x, y)) & \text{if } P_c(x, y) < P_s(x, y). \end{cases} \quad (9.16)$$

Figure 9.13 shows a selected region for microcalcification feature enhancement from a digitized film-mammogram along with the enhanced image using feature-adaptive neighborhood processing. The microcalcification details can be seen more clearly in the enhanced image. The enhanced image using the histogram equalization method is also shown in Figure 9.13 for comparison. A loss of resolution resulting from the saturated regions can be seen in the enhanced image provided by the histogram equalization method.

An adaptive image enhancement method using the first-order derivative information has been used for enhancing specific mammographic features such as stellate lesions, circumscribed masses, and microcalcification (14).

9.2. FREQUENCY DOMAIN FILTERING

Frequency domain filtering methods process an acquired image in the Fourier domain to emphasize or de-emphasize specified frequency components. In general, the frequency components can be expressed in low and high ranges. The low-frequency range components usually represent shapes and blurred structures in the image, while high-frequency information belongs to sharp details, edges, and noise. Thus a low-pass filter with attenuation to high-frequency components would provide image smoothing and noise removal. A high-pass filtering with attenuation to low-frequency extracts edges and sharp details for image enhancement and sharpening effects.

As presented in Chapter 2, an acquired image $g(x, y)$ can be expressed as a convolution of the object $g(x, y)$ with a PSF $h(x, y)$ of a linear spatially invariant imaging system with additive noise $n(x, y)$ as

$$g(x, y) = h(x, y) \otimes f(x, y) + n(x, y) \quad (9.17)$$

The Fourier transform of Equation 9.17 provides a multiplicative relationship of $F(u, v)$, the Fourier transform of the object, and $H(u, v)$, the Fourier transform of the PSF.

$$G(u, v) = H(u, v)F(u, v) + N(u, v) \quad (9.18)$$

where u and v represent frequency domain along x - and y -directions, and $G(u, v)$ and $N(u, v)$ are, respectively, the Fourier transforms of the acquired image $g(x, y)$ and the noise $n(x, y)$.

The object information in the Fourier domain can be recovered by inverse filtering as

$$\hat{F}(u, v) = \frac{G(u, v)}{H(u, v)} - \frac{N(u, v)}{H(u, v)} \quad (9.19)$$

where $\hat{F}(u, v)$ is the restored image in the frequency domain.

The inverse filtering operation represented in Equation 9.19 provides a basis for image restoration in the frequency domain. The inverse Fourier transform of $F(u, v)$ provides the restored image in the spatial domain. The PSF of the imaging system can be experimentally determined or statistically estimated (1).

9.2.1 Wiener Filtering

The image restoration approach presented in Equation 9.19 appears to be simple but poses a number of challenges in practical implementation. Besides the difficulties associated with the determination of the PSF, low values or zeros in $H(u, v)$ cause computational problems. Constrained deconvolution approaches and weighted filtering have been used to avoid the “division by zero” problem in Equation 9.19 (1–3). Wiener filtering is a well-known and effective method for image restoration to perform weighted inverse filtering as

$$\hat{F}(u, v) = \left[\left(\frac{1}{H(u, v)} \right) \left(\frac{|H(u, v)|^2}{|H(u, v)|^2 + \frac{S_n(u, v)}{S_f(u, v)}} \right) \right] G(u, v) \quad (9.20)$$

where $S_f(u, v)$ and $S_n(u, v)$ are, respectively, the power spectrum of the signal and noise.

The Wiener filter, also known as the minimum square error filter, provides an estimate determined by exact inverse filtering if the noise spectrum is zero. In cases of nonzero signal-to-noise spectrum ratio, the division is appropriately weighted. If the noise can be assumed to be spectrally white, Equation 9.20 reduces to a simple parametric filter with a constant K as

$$\hat{F}(u, v) = \left[\left(\frac{1}{H(u, v)} \right) \left(\frac{|H(u, v)|^2}{|H(u, v)|^2 + K} \right) \right] G(u, v). \quad (9.21)$$

In implementing inverse filtering-based methods for image restoration, the major issue is the estimation of the PSF and noise spectra. The estimation of PSF is

dependent on the instrumentation and parameters of the imaging modality. For example, in the echo planar imaging (EPI) sequence method of MR imaging, an image formation process can be described in a discrete representation by (15, 16)

$$g(x, y) = \sum_{x'=0}^{M-1} \sum_{y'=0}^{N-1} f(x', y') H(x', y'; x, y) \quad (9.22)$$

where $g(x, y)$ is the reconstructed image of $M \times N$ pixels, $f(x, y)$ is the ideal image of the object, and $H(x', y'; x, y)$ is the PSF of the image formation process in EPI. The MR signal $s(k, l)$ at a location (k, l) in the k -space for the EPI method can be represented as

$$s(k, l) = \sum_{x=0}^{M-1} \sum_{y=0}^{N-1} f(x, y) A(x, y; k, l) \quad (9.23)$$

where

$$A(x, y; k, l) = e^{-2\pi j((kx/M)+(ly/N)-(\gamma/2\pi)\Delta B_{x,y} t_{k,l})} \quad (9.24)$$

where $\Delta B_{x,y}$ is spatially variant field inhomogeneity and $t_{k,l}$ is the time between the sampling of the k -space location (k, l) and the RF excitation.

With the above representation, the PSF $H(x', y'; x, y)$ can be obtained from the two-dimensional (2-D) inverse FFT of the function $A(x, y; k, l)$ as

$$\begin{aligned} H(x', y'; x, y) &= \sum_{k=0}^{M-1} \sum_{l=0}^{N-1} A(x, y; k, l) e^{2\pi j((kx/M)+ly/N)} \\ &= \sum_{k=0}^{M-1} \sum_{l=0}^{N-1} e^{2\pi j((k(x'-x)/M)+(l(y'-y)/N)-(\gamma/2\pi)\Delta B_{x,y} t_{k,l})}. \end{aligned} \quad (9.25)$$

9.2.2 Constrained Least Square Filtering

The constrained least square filtering method uses optimization techniques on a set of equations representing the image formation process. Equation 9.18 can be rewritten in matrix form as

$$\mathbf{g} = \mathbf{H}\mathbf{f} + \mathbf{n} \quad (9.26)$$

where \mathbf{g} is a column vector representing the reconstructed image $g(x, y)$, \mathbf{f} is a column vector of $MN \times 1$ dimension, representing the ideal image $f(x, y)$, and \mathbf{n} represents the noise vector. The PSF is represented by the matrix \mathbf{H} of $MN \times MN$ elements.

For image restoration using the above equation, an estimate $\hat{\mathbf{f}}$ needs to be computed such that the mean-square error between the ideal image and the estimated image is minimized. The overall problem may not have a unique solution. Also, small variations in the matrix \mathbf{H} may have significant impact on the noise content of the restored image. To overcome these problems, regularization methods involving constrained optimization techniques are used. Thus, the optimization process is subjected to specific constraints such as smoothness to avoid noisy solutions for the vector $\hat{\mathbf{f}}$. The smoothness constraint can be derived from the Laplacian for the estimated image. Using the theory of random variables, the optimization process is defined to estimate $\hat{\mathbf{f}}$ such that the mean-square error, e^2 given by

$$e^2 = \text{Trace } E\{(\mathbf{f} - \hat{\mathbf{f}})\mathbf{f}^\dagger\}$$

is minimized subject to the smoothness constraint involving the minimization of the roughness or Laplacian of the estimated image as

$$\min \{ \hat{\mathbf{f}}^t [\mathbf{C}]^t [\mathbf{C}] \hat{\mathbf{f}} \}$$

where

$$[\mathbf{C}] = \begin{bmatrix} 1 & & & & & \\ -2 & 1 & & & & \\ 1 & -2 & 1 & & & \\ & 1 & -2 & & & \\ & & 1 & . & & \\ & & & . & 1 & \\ & & & & -2 & \\ & & & & & 1 \end{bmatrix}. \quad (9.27)$$

It can be shown that the estimated image $\hat{\mathbf{f}}$ can be expressed as (4)

$$\hat{\mathbf{f}} = \left([\mathbf{H}]^t [\mathbf{H}] + \frac{1}{\lambda} [\mathbf{C}]^t [\mathbf{C}] \right)^{-1} [\mathbf{H}]^t \mathbf{g} \quad (9.28)$$

where λ is a Lagrange multiplier.

9.2.3 Low-Pass Filtering

The ideal low-pass filter suppresses noise and high-frequency information providing a smoothing effect to the image. A 2-D low-pass filter function $H(u, v)$ is multiplied with the Fourier transform $G(u, v)$ of the image to provide a smoothed image as

$$\hat{F}(u, v) = H(u, v)G(u, v) \quad (9.29)$$

where $\hat{F}(u, v)$ is the Fourier transform of the filtered image $\hat{f}(x, y)$ that can be obtained by taking an inverse Fourier transform.

An ideal low-pass filter can be designed by assigning a frequency cutoff value, ω_0 . The frequency cutoff value can also be expressed as the distance D_0 from the origin in the Fourier (frequency) domain.

$$H(u, v) = \begin{cases} 1 & \text{if } D(u, v) \leq D_0 \\ 0 & \text{otherwise} \end{cases} \quad (9.30)$$

where $D(u, v)$ is the distance of a point in the Fourier domain from the origin representing the dc value.

An ideal low-pass filter has sharp cutoff characteristics in the Fourier domain, causing a rectangular window for the pass band. From Chapter 2, it can be shown that a rectangular function in the frequency domain provides a sinc function in the spatial domain. Also, the multiplicative relationship of the filter model in Equation 9.29 causes a convolution operation in the spatial domain. The rectangular pass-band window in the ideal low-pass filter causes ringing artifacts in the spatial domain. To reduce ringing artifacts, the pass band should have a smooth fall-off characteristic.

A Butterworth low-pass filter of n th order can be used to provide smoother fall-off characteristics and is defined as

$$H(u, v) = \frac{1}{1 + [D(u, v)/D_0]^{2n}}. \quad (9.31)$$

As the order n increases, the fall-off characteristics of the pass band become sharper. Thus, a first-order Butterworth filter provides the least amount of ringing artifacts in the filtered image.

A Gaussian function is also commonly used for low-pass filtering to provide smoother fall-off characteristics of the pass band and is defined by

$$H(u, v) = e^{-D^2(u, v)/2\sigma^2} \quad (9.32)$$

where $D(u, v)$ is the distance from the origin in the frequency domain and σ represents the standard deviation of the Gaussian function that can be set to the cutoff distance D_0 in the frequency domain.

In the above case, the gain of the filter is down to 0.607 of its maximum value at the cutoff frequency. Figure 9.14 shows a low-pass filter function with Gaussian window-based roll-off characteristics and the results of low-pass filtering of the MR brain image shown in Figure 9.1.

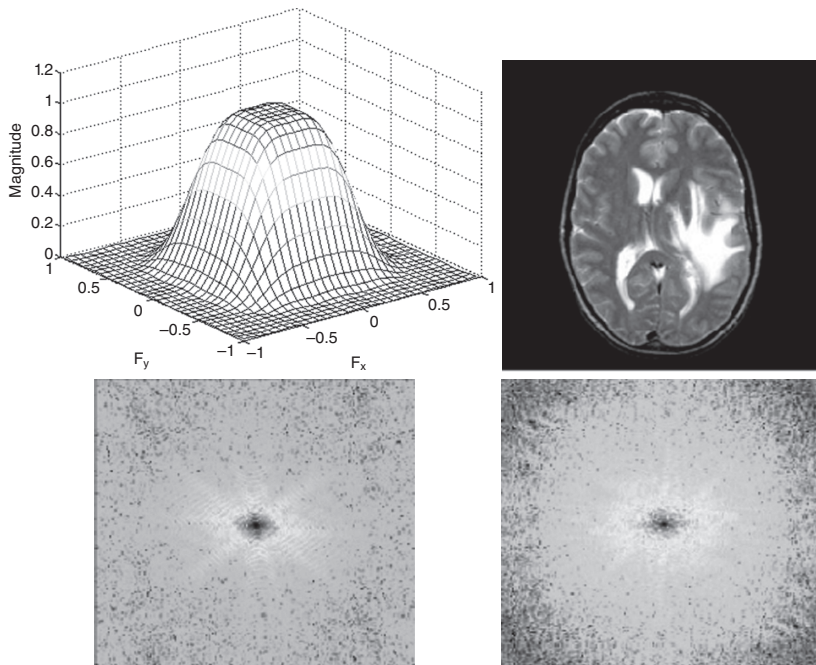


Figure 9.14 From top left clockwise: A low-pass filter function $H(u, v)$ in the Fourier domain, the low-pass filtered MR brain image, the Fourier transform of the original MR brain image shown in Figure 9.1, and the Fourier transform of the low-pass filtered MR brain image.

9.2.4 High-Pass Filtering

High-pass filtering is used for image sharpening and extraction of high-frequency information such as edges. The low-frequency information is attenuated or blocked depending on the design of the filter. An ideal high-pass filter has a rectangular window function for the high-frequency pass band. Since the noise in the image usually carries high-frequency components, high-pass filtering shows the noise along with edge information. An ideal 2-D high-pass filter with a cutoff frequency at a distance D_0 from the origin in the frequency domain is defined as

$$H(u, v) = \begin{cases} 0 & \text{if } D(u, v) \geq D_0 \\ 1 & \text{otherwise} \end{cases}. \quad (9.33)$$

As described above for an ideal low-pass filter, the sharp cutoff characteristic of the rectangular window function in the frequency domain as defined in Equation 9.33 causes the ringing artifacts in the filtered image in the spatial domain. To avoid ringing artifacts, filter functions with smoother fall-off characteristics such as Butterworth and Gaussian are used. A Butterworth high-pass filter of n th order is defined in the frequency domain as

$$H(u, v) = \frac{1}{1 + [D_0 / D(u, v)]^{2n}}. \quad (9.34)$$

A Gaussian high-pass filter is defined in the frequency domain as

$$H(u, v) = 1 - e^{-D^2(u, v)/2\sigma^2}. \quad (9.35)$$

Figure 9.15 shows a Gaussian high-pass filter function and the results of high-pass filtering of the MR brain image shown in Figure 9.1.

9.2.5 Homomorphic Filtering

The filtering model described above utilizes a single function or property (such as brightness) of the image. However, in homomorphic systems, the image formation can be described as a multiplication of two or more functions. For example, an image acquired by a photographic camera can be expressed as

$$f(x, y) = i(x, y)r(x, y) \quad (9.36)$$

where $i(x, y)$ and $r(x, y)$, respectively, represent the illumination and reflectance for a spatial point (x, y) in the image. In general, a two-function-based homomorphic system can be described as

$$f(x, y) = f_1(x, y)f_2(x, y) \quad (9.37)$$

where $f_1(x, y)$ and $f_2(x, y)$, respectively, represent two properties of the image.

The multiplicative relationship of two functions in Equation 9.37 can be converted into an additive relationship by applying a logarithmic operator as

$$g(x, y) = \ln f(x, y) = \ln f_1(x, y) + \ln f_2(x, y). \quad (9.38)$$

Homomorphic filtering is a method to perform frequency filtering in the logarithmic transform domain. Since the filtering is done in the frequency domain of the log of

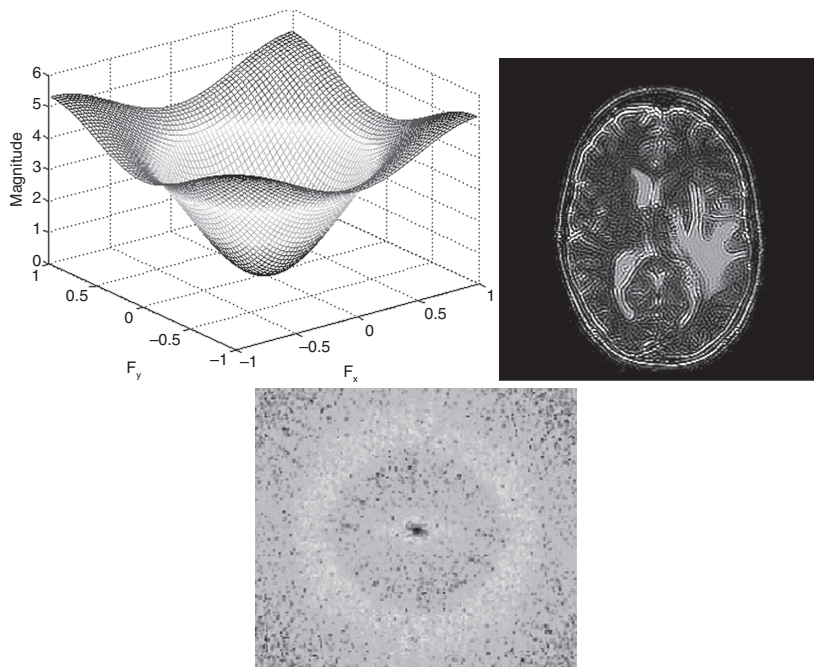


Figure 9.15 From top left clockwise: A high-pass filter function $H(u, v)$ in the Fourier domain, the high-pass filtered MR brain image, and the Fourier transform of the high-pass filtered MR brain image.

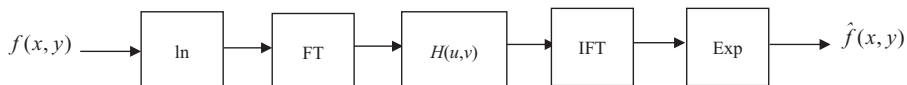


Figure 9.16 A schematic block diagram of homomorphic filtering method.

the image, after the filtering operation, an exponential operation has to be performed to get back to the spatial image domain. A block diagram of the homomorphic filtering method is shown in Figure 9.16.

The Fourier transform of Equation 9.38 provides

$$G(u, v) = F_1(u, v) + F_2(u, v). \quad (9.39)$$

With the application of a filter function $H(u, v)$ in the frequency domain, the filtered version can be expressed as

$$S(u, v) = H(u, v)G(u, v) = H(u, v)F_1(u, v) + H(u, v)F_2(u, v). \quad (9.40)$$

Taking inverse Fourier transform on Equation 9.40 provides

$$\begin{aligned} s(x, y) &= F^{-1}\{H(u, v)F_1(u, v)\} + F^{-1}\{H(u, v)F_2(u, v)\} \\ &= f'_1(x, y) + f'_2(x, y). \end{aligned} \quad (9.41)$$

Finally, an exponential operation is applied to obtain the filtered image $\hat{f}(x, y)$ in the spatial image domain as

$$\hat{f}(x, y) = e^{s(x, y)} = \hat{f}_1(x, y)\hat{f}_2(x, y). \quad (9.42)$$

If a model for the identification of functions, $f_1(x, y)$ and $f_2(x, y)$, is available, two different filter functions can be applied separately on the corresponding representation of each function. Typical filter functions such as Butterworth or Gaussian can be applied to implement homomorphic filter function $H(u, v)$ in the Fourier transform of the log domain of the image. In the absence of an imaging model, heuristic knowledge can be used to implement homomorphic filtering. For example, $f_1(x, y)$ and $f_2(x, y)$ components can represent, respectively, low- and high-frequency components in the image. A circularly symmetric homomorphic filter function can then be designed, as shown in Figure 9.17 (1).

A Gaussian high-pass filter function can then be used with some modification for implementation in the homomorphic filtering scheme for image sharpening as (1)

$$H(u, v) = (\gamma_H - \gamma_L)[1 - e^{c(D^2(u, v)/\sigma^2)}] + \gamma_L \quad (9.43)$$

where c is the parameter to control the sharpness effect in the filtered image. The MR brain image sharpened by homomorphic filtering using a circularly symmetric function obtained from the function shown in Figure 9.17 is shown in Figure 9.18.

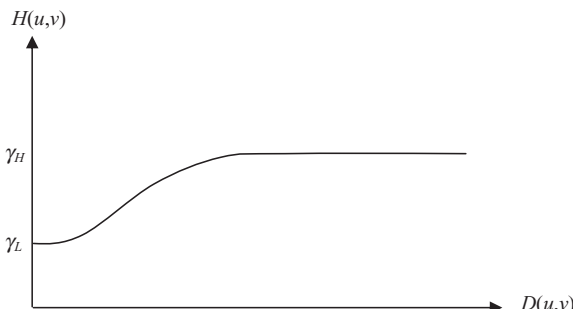


Figure 9.17 A circularly symmetric filter function for homomorphic filtering.



Figure 9.18 The enhanced MR brain image obtained by homomorphic filtering using a circularly symmetric function shown in Equation 9.43.

9.3. WAVELET TRANSFORM FOR IMAGE PROCESSING

As described in Chapter 2, wavelet transform provides a complete localization of spatio-frequency features in the image. Wavelet transform decomposes an image into a set of linearly weighted orthonormal basis functions through scaling and shifting operations. For wavelet transform analysis, a set of orthonormal basis functions is generated by scaling and translation of the mother wavelet $\psi(t)$ and the scaling function $\phi(t)$. Using the scaling operations, the multiresolution approach of the wavelet transform provides localization and representation of different frequencies in the image at different scales.

The wavelet functions with scaling and translations form an orthonormal basis in $L^2(\mathbf{R})$. The wavelet-spanned multiresolution subspace satisfies the relation

$$\begin{aligned} V_{j+1} &= V_j \oplus W_j \\ &= V_{j-1} \oplus W_{j-1} \oplus W_j \\ &= V_{j-2} \oplus W_{j-2} \oplus W_{j-1} \oplus W_j \end{aligned}$$

where \oplus denotes the union operation of subspaces, and

$$L^2(\mathbf{R}) = \dots \oplus W_{-2} \oplus W_{-1} \oplus W_0 \oplus W_1 \oplus W_2 \oplus \dots \quad (9.44)$$

where the original space V_{j+1} is divided into V_j and W_j spectral subspaces as the output of the low-pass and high-pass filters, respectively. These subspaces are then further decomposed into smaller spectral bands.

The wavelet functions span the orthogonal complement spaces with scaling and wavelet filter coefficients that are related as

$$h_\psi(n) = (-1)^n h_\phi(1-n). \quad (9.45)$$

As described in Chapter 2, an arbitrary square summable sequence $x[n]$ representing a signal in the time or space domain is expressed as

$$x[n] \in L^2(\mathbf{R}). \quad (9.46)$$

The discrete signal $x[n]$ is decomposed into wavelet transform domain to obtain coefficients $X[k]$ as

$$x[n] = \sum_{k \in Z} \langle \varphi_k[l] x[l] \rangle \varphi_k[n] = \sum_{k \in Z} X[k] \varphi_k[n]$$

where

$$\begin{aligned} \varphi_{2k}[n] &= h_0[2k - n] = g_0[n - 2k] \\ \varphi_{2k+1}[n] &= h_1[2k - n] = g_1[n - 2k] \end{aligned}$$

and

$$\begin{aligned} X[2k] &= \langle h_0[2k - l], x[l] \rangle \\ X[2k + 1] &= \langle h_1[2k - l], x[l] \rangle. \end{aligned} \quad (9.47)$$

In Equation 9.47, the orthonormal bases $\phi_k[n]$ are expressed as low-pass and high-pass filters for decomposition and reconstruction of a signal using the quadrature-mirror filter theory. The low-pass and high-pass filters for signal decomposition or

analysis are expressed, respectively, as h_0 and h_1 , while g_0 and g_1 are, respectively, the low-pass and high-pass filters for signal reconstruction or synthesis. A perfect reconstruction of the signal can be obtained from the wavelet coefficients as

$$\begin{aligned} x[n] &= \sum_{k \in \mathbb{Z}} X[2k]\phi_{2k}[n] + \sum_{k \in \mathbb{Z}} X[2k+1]\phi_{2k+1}[n] \\ &= \sum_{k \in \mathbb{Z}} X[2k]g_0[n-2k] + \sum_{k \in \mathbb{Z}} X[2k+1]g_1[n-2k]. \end{aligned} \quad (9.48)$$

Figure 9.19a (reproduced from Chapter 2) shows a schematic diagram of multiresolution signal decomposition using low-pass (H_0) and high-pass (H_1) decomposition filters to obtain wavelet coefficients. Figure 9.19b shows a schematic diagram of signal reconstruction from wavelet coefficients using low-pass (G_0) and high-pass (G_1) reconstruction filters. As described in Chapter 2, an image can be analyzed using one-dimensional (1-D) wavelet transform with low-pass and high-pass decomposition filters in multiresolution space for image processing applications. The image is first sampled along the rows and then along the columns for analysis using 1-D low-pass and high-pass filters. The image, at resolution 2^{j+1} , represented by A_{j+1} , is first low-pass and then high-pass filtered along the rows. The result of each filtering process is subsampled. Next, the subsampled results are low-pass and high-pass filtered along each column. The results of these filtering processes are again subsampled. The frequency band denoted by A_j in Figure 9.20 is referred to as the low-low-frequency band. It contains the scaled low-frequency information. The frequency bands labeled D_j^1 , D_j^2 , and D_j^3 denote the detail information. They are referred to as low-high, high-low, and high-high-frequency bands, respectively. This analysis can be iteratively applied to an image for further decompose into narrower frequency bands, that is, each frequency band can be further decomposed into four

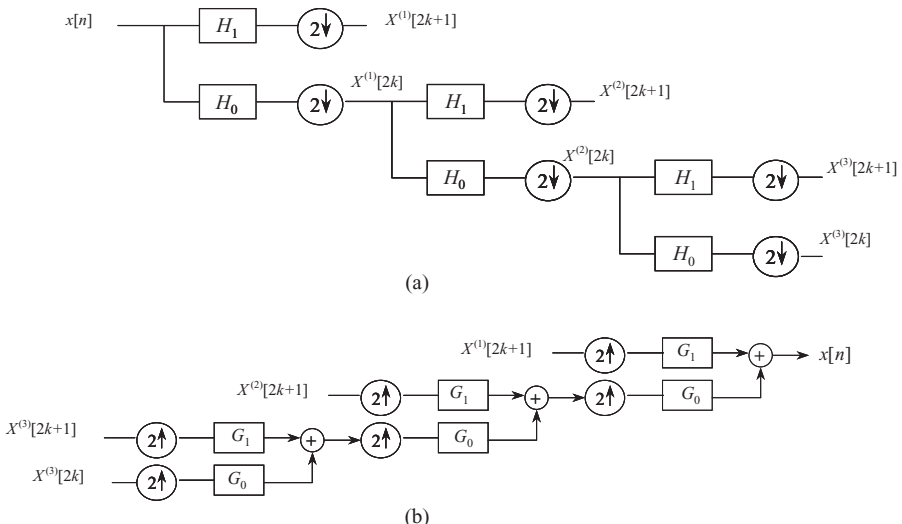


Figure 9.19 (a) A multiresolution signal decomposition using wavelet transform and (b) the reconstruction of the signal from wavelet transform coefficients.

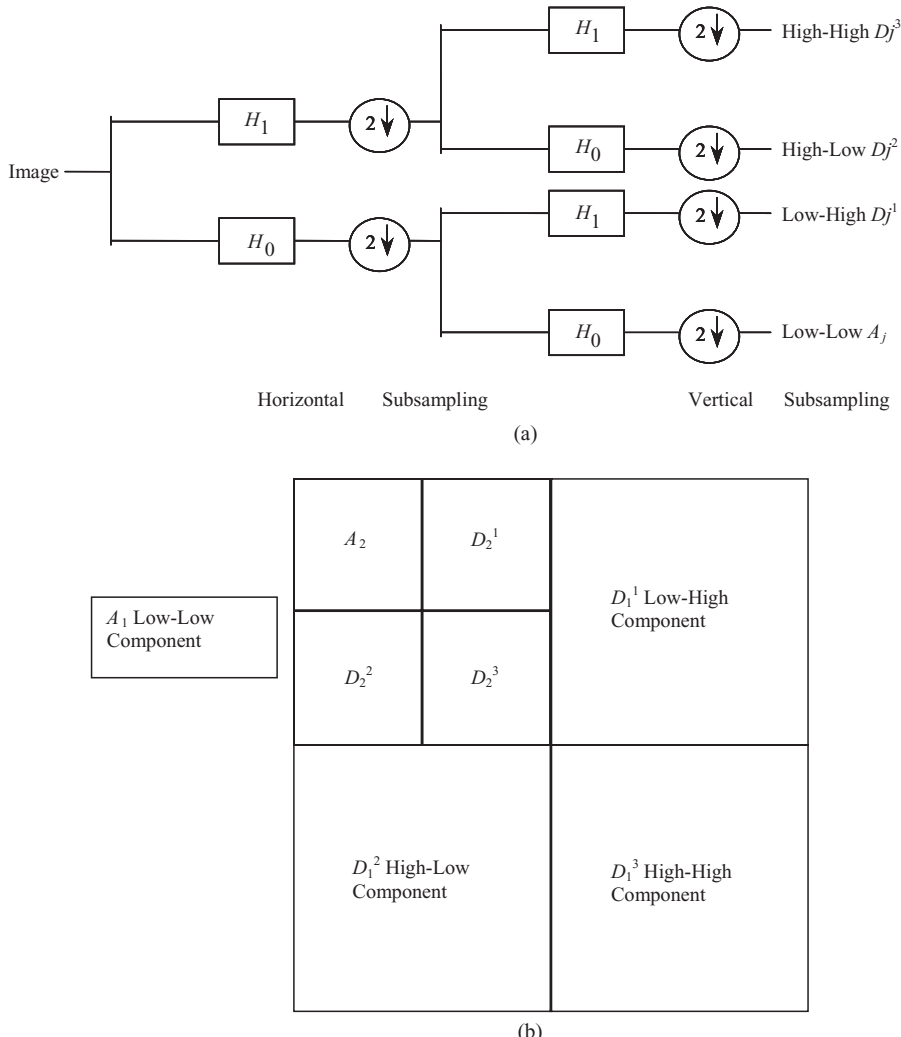


Figure 9.20 (a) Multiresolution decomposition of an image using the wavelet transform. (b) Wavelet transform-based image decomposition: the original resolution image ($N \times N$) is decomposed into four low-low A_1 , low-high D_1^1 , high-low D_1^2 , and high-high D_1^3 images each of which is subsampled to resolution $[(N/2) \times (N/2)]$. The low-low image is further decomposed into four images of $[(N/4) \times (N/4)]$ resolution each in the second level of decomposition. For a full decomposition, each of the “Detail” component can also be decomposed into four sub-images with $[(N/4) \times (N/4)]$ resolution each.

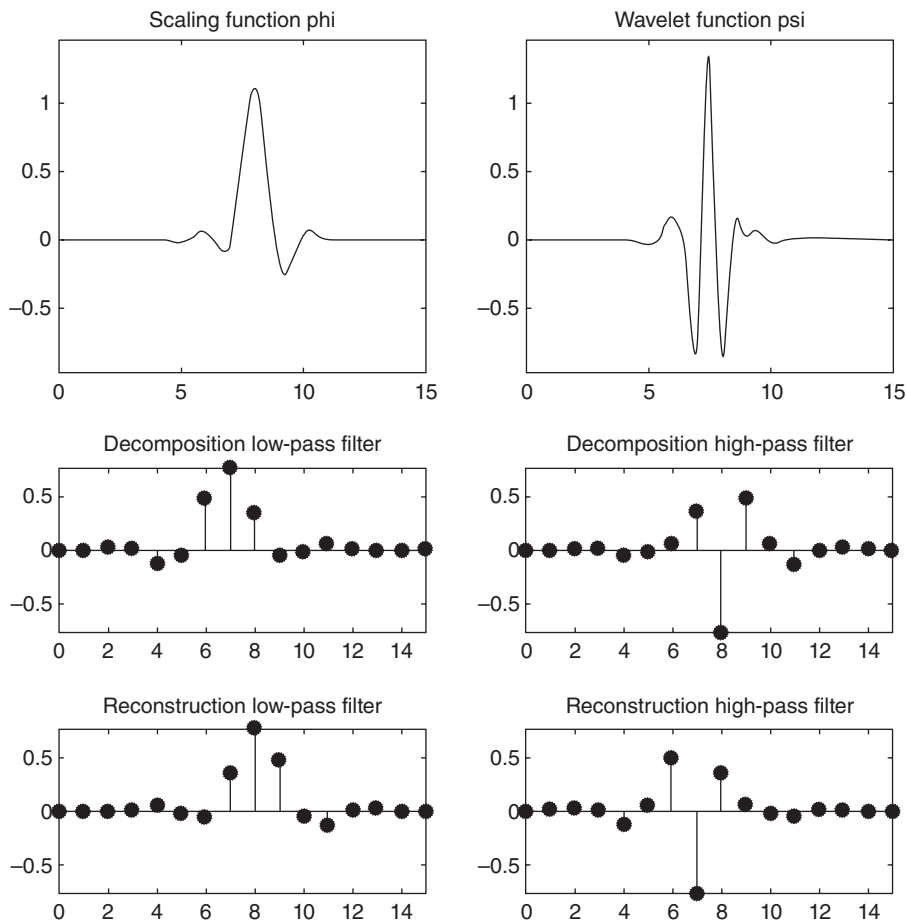


Figure 9.21 A least asymmetric wavelet with eight coefficients.

narrower bands. Each level of decomposition reduces the resolution by a factor of two. The multiscale framework of signal decomposition into narrower frequency bands is also called wavelet packet analysis.

The “least asymmetric” wavelets were designed by Daubechies (17) for applications in signal and image processing. A least asymmetric wavelet is shown in Figure 9.21 with the coefficients of the corresponding low-pass and high-pass filters given in Table 9.1.

9.3.1 Image Smoothing and Enhancement Using Wavelet Transform

The wavelet transform provides a set of coefficients representing the localized information in a number of frequency bands. A popular method for denoising and smoothing is to threshold the coefficients in those bands that have high probability

TABLE 9.1 The Coefficients for the Corresponding Low-Pass and High-Pass Filters for the Least Asymmetric Wavelet

N	High-pass	Low-pass
0	-0.107148901418	0.045570345896
1	-0.041910965125	0.017824701442
2	0.703739068656	-0.140317624179
3	1.136658243408	-0.421234534204
4	0.421234534204	1.136658243408
5	-0.140317624179	-0.703739068656
6	-0.017824701442	-0.041910965125
7	0.045570345896	0.107148901418

of noise and then reconstruct the image using reconstruction filters. Reconstruction filters, as described in Equation 9.48, can be derived from the decomposition filters using the quadrature-mirror theory (17–20). The reconstruction process integrates information from specific bands with successive upscaling of resolution to provide the final reconstructed image at the same resolution as the input image. If certain coefficients related to the noise or noise-like information are not included in the reconstruction process, the reconstructed image shows a reduction of noise and smoothing effects.

Wavelet coefficients are correlated with specific spatio-frequency features in the image (21, 22). A specific feature can be eliminated if the respective wavelet coefficient(s) in the wavelet transform domain are thresholded and then the image is reconstructed using nonthresholded coefficients. Similarly, a specific feature can be enhanced if the corresponding wavelet coefficients are strengthened (multiplied by appropriate gain factor while others may be threshold and normalized) in the wavelet transform domain, and then the image is reconstructed from using modified wavelet coefficients with an appropriate interpolation method (23, 24). For image denoising or smoothing, hard or soft thresholding methods may be applied in the wavelet transform domain. With the hard thresholding method, all coefficients below the predetermined threshold are set to zero as

$$\omega_T(X) = \begin{cases} X & \text{if } |X| > T \\ 0 & \text{if } |X| \leq T \end{cases} \quad (9.49)$$

where $\omega_T(X)$ represents modified coefficient value for thresholding the wavelet coefficient X at the threshold T .

In the soft thresholding method, the nonthresholded coefficients are rearranged to the range of 0 to maximum value as

$$\omega_T(X) = \begin{cases} X - T & \text{if } |X| \geq T \\ X + T & \text{if } |X| \leq -T \\ 0 & \text{if } |X| < T \end{cases}. \quad (9.50)$$

Monotonically increasing or piecewise linear enhancement functions can be used in rescaling and thresholding wavelet coefficients in the wavelet transform domain

for specific feature enhancement (25–27). Laine et al. (26) used a simple piecewise linear enhancement function to modify wavelet coefficients for feature enhancement as

$$E(X) = \begin{cases} X - (K-1)T & \text{if } X < -T \\ KX & \text{if } |X| \leq T \\ X + (K-1)T & \text{if } X > T \end{cases} \quad (9.51)$$

where $E(X)$ represents enhanced coefficient value for the wavelet coefficient X at the threshold T .

As can be seen in Figure 9.22, the coefficients available in the low-high, high-low, and high-high-frequency bands in the decomposition process provide edge-related information that can be emphasized in the reconstruction process for image sharpening (10, 22). Figure 9.23 shows a smoothed version of the MR brain image reconstructed using all bands, except the high-high-frequency band. Figure 9.24 shows an image that is reconstructed using the high-high-frequency band information only.

It is difficult to discriminate image features from noise based on the spatial distribution of gray values. The noise, which is usually of a high-frequency nature, should be de-emphasized when other high-frequency features of interest, such as edges, are enhanced. A useful distinction between the noise and image features may be made, if some knowledge about the processed image features and their behavior is known a priori. This points out the need for some partial image analysis that must be performed before the image enhancement operations are performed. Thus, an intelligent or knowledge-based feature enhancement may provide better

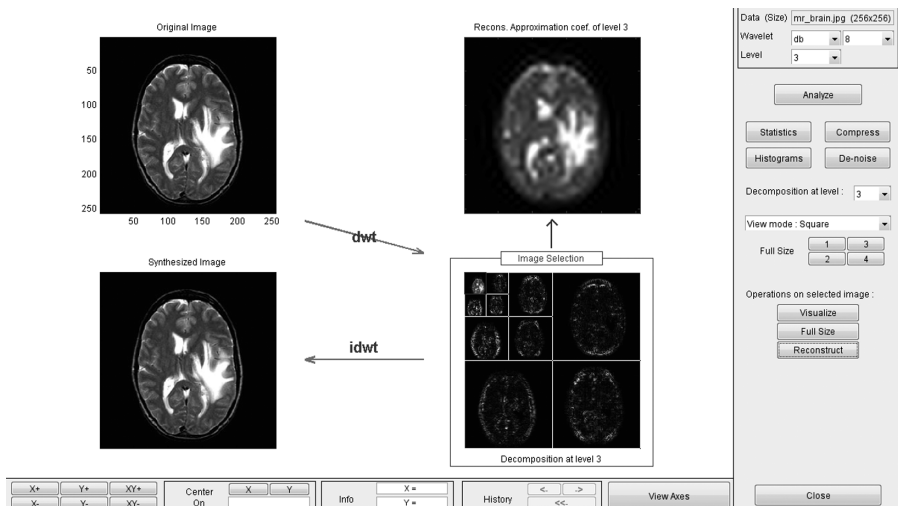


Figure 9.22 Three-level wavelet decomposition of the MR brain image (top left) is shown at the bottom right with inverse discrete wavelet transform shown at bottom left. A reconstruction from low-low pass-band decomposition at the third level is shown at the top right.

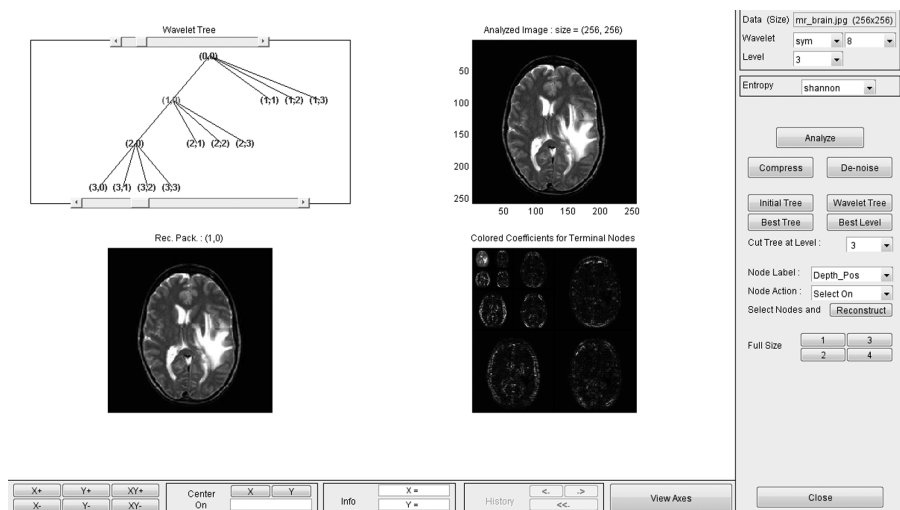


Figure 9.23 The MR brain image of Figure 9.1 (top right) reconstructed from the low-low-frequency band at the first decomposition level (node [1, 0] in the wavelet tree) is shown at the bottom left with three levels of wavelet decomposition (bottom right).



Figure 9.24 The MR brain image of Figure 9.1 reconstructed from the low-high, high-low, and high-high-frequency bands using the wavelet decomposition shown in Figure 9.21.

enhancement. An example is provided above for the enhancement of microcalcification features in X-ray mammography. A scale-based diffusive image filtering method is used for MR images for image enhancement and denoising while preserving high-frequency-based fine structures (25–27).

9.4. EXERCISES

- Why are image smoothing and image sharpening operations important in medical image processing and analysis?
- What is the difference between image smoothing and image sharpening?

- 9.2.** What is the difference between spatial and frequency filtering methods? Compare the advantages of both types of methods.
- 9.3.** Does median filtering provide better image smoothing and denoising than weighted averaging? Apply both methods in MATLAB on a CT brain image and compare their results.
- 9.4.** Use the following image enhancement methods in MATLAB on a T_1 -weighted MR brain image and comment on the contrast of features in enhanced images:
- Histogram equalization
 - Sobel gradient masks
 - Laplacian gradient mask
 - Local histogram equalization
- 9.5.** Repeat Exercise 9.4 for an X-ray mammography image and comment on the results on contrast enhancement for each method. Do you observe similar effects of feature enhancement on the mammography image as you observed for the MR brain image in Exercise 9.4?
- 9.6.** Use the image selected in Exercise 9.4 for Gaussian high-pass filtering for image sharpening. Compare the filtered image with the enhanced image obtained using Laplacian mask.
- 9.7.** Apply a parametric Weiner filtering method on the image selected in Exercise 9.5 and compare the results for three choices of the parameter K . Assume a Gaussian blur function with a variance of 9 pixels to compute a PSF. What is the effect of using different values of the parameter K on the output image?
- 9.8.** Add Gaussian noise to the mammography image used in Exercise 9.5 using the “noise” function in MATLAB. Repeat Exercise 9.5 on the noisy image and compare restored images with those obtained in Exercise 9.5.
- 9.9.** Use a brain image for wavelet-based three-level decomposition using the following wavelets (level 4) in the MATLAB environment:
- HAAR
 - db6
 - db8
 - sym4
- 9.10.** Using the decomposition tree in the MATLAB environment, reconstruct the image using the following subbands and compare the results with respect to visible features:
- Low-low-low
 - High-high-high
 - All bands except low-low-low
- 9.11.** Repeat Exercise 9.13 for the X-ray mammography image selected in Exercise 9.5. Compare wavelet-based image enhancement results with those obtained from Gaussian low-pass and high-pass frequency filtering in Exercise 9.5.

9.5. REFERENCES

1. R.C. Gonzalez and R.E. Woods, *Digital Image Processing*, Prentice Hall, Englewood Cliffs, NJ, 2002.
2. A.K. Jain, *Fundamentals of Digital Image Processing*, Prentice Hall, Englewood Cliffs, NJ, 1989.
3. R. Jain, R. Kasturi, and B.G. Schunck, *Machine Vision*, McGraw-Hill, New York, 1995.
4. A. Rosenfeld and A.V. Kak, *Digital Picture Processing*, Volumes 1 and 2, 2nd Edition, Academic Press, Orlando, FL, 1982.
5. J.C. Russ, *The Image Processing Handbook*, 2nd Edition, CRC Press, Boca Raton, FL, 1995.
6. R.J. Schalkoff, *Digital Image Processing and Computer Vision*, John Wiley & Sons, New York, 1989.
7. Y.H. Kao and J.R. MacFall, "Correction of MR-k space data corrupted by spike noise," *IEEE Trans. Med. Imaging*, Vol. 19, pp. 671–680, 2000.
8. O.A. Ahmed and M.M. Fahmy, "NMR signal enhancement via a new time-frequency transform," *IEEE Trans. Med. Imaging*, Vol. 20, pp. 1018–1025, 2001.
9. C. Goutte, F.A. Nielson, and L.K. Hansen, "Modeling of hemodynamic response in fMRI using smooth FIR filters," *IEEE Trans. Med. Imaging*, Vol. 19, pp. 1188–1201, 2000.
10. S. Zaroubi and G. Goelman, "Complex denoising of MR data via wavelet analysis: Applications for functional MRI," *Magn. Reson. Imaging*, Vol. 18, pp. 59–68, 2000.
11. G.W. Davis and S.T. Wallenlager, "Improvement of chest region CT images through automated gray-level remapping," *IEEE Trans. Med. Imaging*, Vol. MI-5, pp. 30–35, 1986.
12. S.M. Pizer, J.B. Zimmerman, and E.V. Staab, "Adaptive gray-level assignment in CT scan display," *J. Comput. Assist. Tomogr.*, Vol. 8, pp. 300–306, 1984.
13. A.P. Dhawan and E. LeRoyer, "Mammographic feature enhancement by computerized image processing," *Comput. Methods Programs Biomed.*, Vol. 27, pp. 23–29, 1988.
14. J.K. Kim, J.M. Park, K.S. Song, and H.W. Park, "Adaptive mammographic image enhancement using first derivative and local statistics," *IEEE Trans. Med. Imaging*, Vol. 16, pp. 495–502, 1997.
15. G. Chen, H. Avram, L. Kaufman, J. Hale, and D. Kramer, "T2 restoration and noise suppression of hybrid MR images using Wiener and linear prediction techniques," *IEEE Trans. Med. Imaging*, Vol. 13, pp. 667–676, 1994.
16. P. Munger, G.R. Crelier, T.M. Peters, and G.B. Pike, "An inverse problem approach to the correction of distortion in EPI images," *IEEE Trans. Med. Imaging*, Vol. 19, pp. 681–689, 2000.
17. I. Daubechies, *Ten Lectures on Wavelets*, Society for Applied Mathematics, Philadelphia, 1992.
18. S. Mallat, "A theory for multiresolution signal decomposition: The wavelet representation," *IEEE Trans. Pattern Anal. Mach. Intell.*, Vol. 11, No. 7, pp. 674–693, 1989.
19. S. Mallat, "Wavelets for a vision," *Proc. IEEE*, Vol. 84, No. 4, pp. 604–614, 1996.
20. M. Vetterli and J. Kovacevic, *Wavelets and Subband Coding*, Prentice Hall, Englewood Cliffs, 1995.
21. A. Bovik, M. Clark, and W. Geisler, "Multichannel texture analysis using localized spatial filters," *IEEE Trans. Pattern Anal. Mach. Intell.*, Vol. 12, pp. 55–73, 1990.
22. J.B. Weaver, X. Yansun, D.M. Healy Jr., and L.D. Cromwell, "Filtering noise from images with wavelet transforms," *Mag. Reson. Med.*, Vol. 21, No. 2, pp. 288–295, 1991.
23. A.P. Pentland, "Interpolation using wavelet bases," *IEEE Trans. Pattern Anal. Mach. Intell.*, Vol. 16, No. 4, pp. 410–414, 1994.
24. M-H. Yaou and W-T. Chang, "Fast surface interpolation using multiresolution wavelet transform," *IEEE Trans. Pattern Anal. Mach. Intell.*, Vol. 16, No. 7, pp. 673–688, 1994.
25. P.K. Saha and J.K. Udupa, "Scale-based diffusive image filtering preserving boundary sharpness and fine structures," *IEEE Trans. Med. Imaging*, Vol. 20, pp. 1140–1155, 2001.
26. A. Laine, "Wavelets in spatial processing of biomedical images," *Annu. Rev. Biomed. Eng.*, Vol. 2, pp. 511–550, 2000.
27. M. Unser, A. Aldroubi, and A. Laine, "IEEE transactions on medical imaging," Special Issue on Wavelets in Medical Imaging, 2003.